

Electronic Supplementary Information (ESI)

Self-assembled one-dimensional MnO_2 @Zeolitic Imidazolate Framework-8 nanostructures for highly efficient arsenite removal

Meipeng Jian,^a Huan Wang,^b Ruiping Liu,^{*b} Jiuhui Qu,^b Huanting Wang,^a and Xiwang Zhang^{*a}

^aDepartment of Chemical Engineering, Monash University, Clayton, Victoria 3800, Australia

^bKey Laboratory of Drinking Water Science and Technology, Research Center for Eco-Environmental Sciences, Chinese Academy of Sciences (CAS), Beijing 100085, China

Correspondence information:

Prof. Ruiping Liu,

Tel: +86 10 6284 9160, E-mail address: liuruiping@rcees.ac.cn

Prof. Xiwang Zhang,

Tel: +61 3 9905 1867, E-mail address: xiwang.zhang@monash.edu

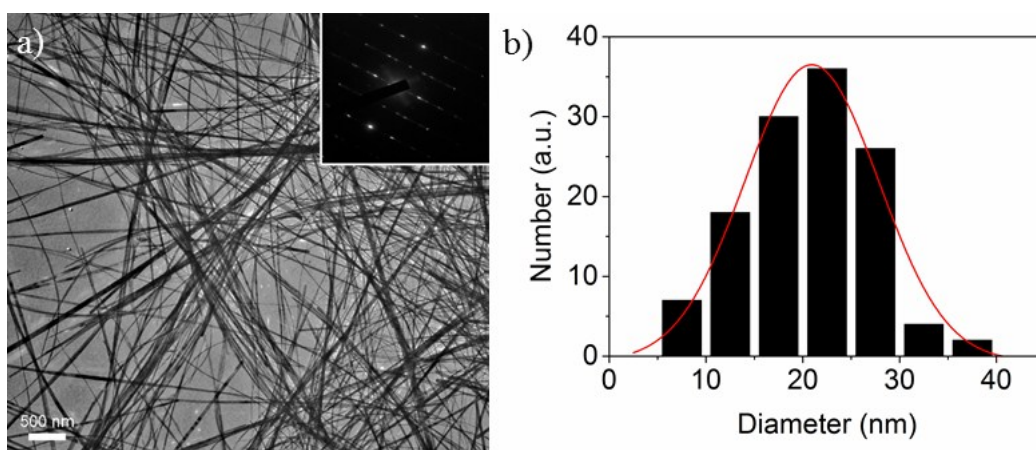


Figure S1 (a) TEM image and (b) diameter distribution histogram of as-prepared β -MnO₂ NWs, inset in (a) showing the corresponding SAED pattern. The red curve based on the Gaussian fitting of the data.

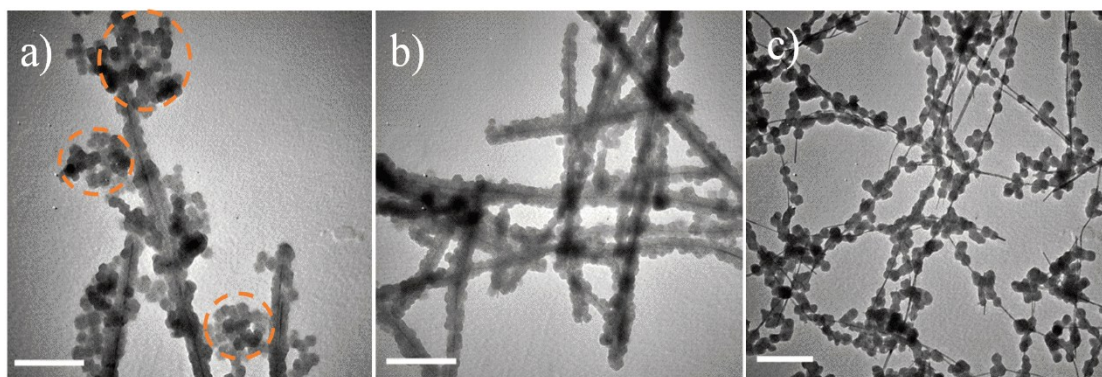


Figure S2 TEM images of as-prepared samples affected by (a) insufficient, (b) moderate and (c) excess MnO_2 NWs additions. Scale bars: 500 nm.

From Figure S2, it is demonstrated that ZIF-8 nanocrystals preferentially coated on the surface of $\beta\text{-MnO}_2$ NWs and formed in solution until completely covered. The content of $\beta\text{-MnO}_2$ NWs in the solution plays an important role in preparing uniform $\text{MnO}_2@\text{ZIF-8}$ NWs. When low concentration of $\beta\text{-MnO}_2$ NWs (1 mg mL^{-1}) was used, a significant amount of ZIF-8 nanocrystals will independently nucleate and agglomerately grow in the solution (orange circles). In contrast, the surface of each $\beta\text{-MnO}_2$ NWs is incompletely coated by ZIF-8 nanocrystals when a high content of $\beta\text{-MnO}_2$ NWs added (3 mg mL^{-1}).

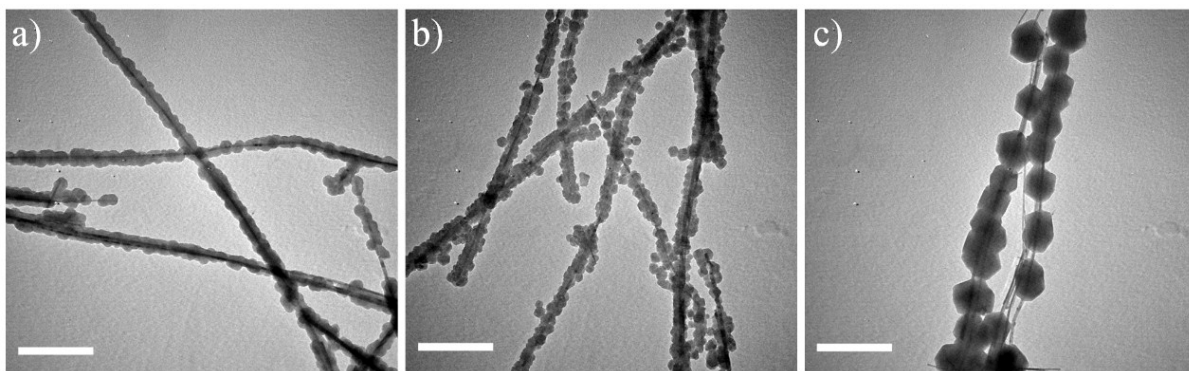


Figure S3. TEM images of $\text{MnO}_2@\text{ZIF-8}$ NWs with tuning the thickness. Scale bars: 500 nm.

The $\text{MnO}_2@\text{ZIF-8}$ NWs with different thicknesses can be obtained by simply varying 2-MeIm ligand concentrations from 0.2 M to 1.6 M to obtain the different sizes of ZIF-8 particles.

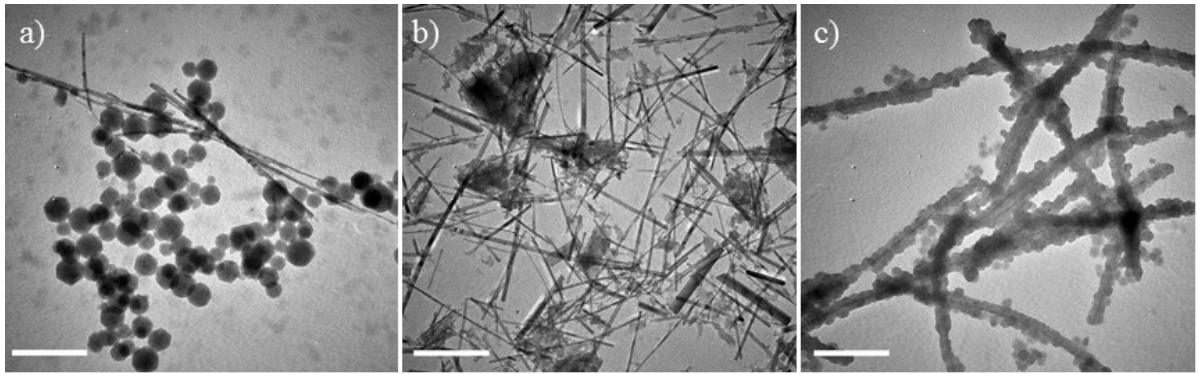


Figure S4. TEM image of $\text{MnO}_2@ZIF-8$ NWs encapsulating in aqueous solution (a), DMF (b) and ethanol solvent (c). Scale bars: 500 nm.

Figure S4 shows that the ZIF-8 particles fail to grow on the surface of MnO_2 NWs to form well-defined core-shell structures in water, instead, ZIF-8 randomly formed in the solution. Moreover, in DMF solvent, the products did not appear to be better even though we purposely increase the concentration of ZIF-8 precursors. However, $\text{MnO}_2@ZIF-8$ NWs assembled in ethanol show a well-defined morphology like that in methanol.

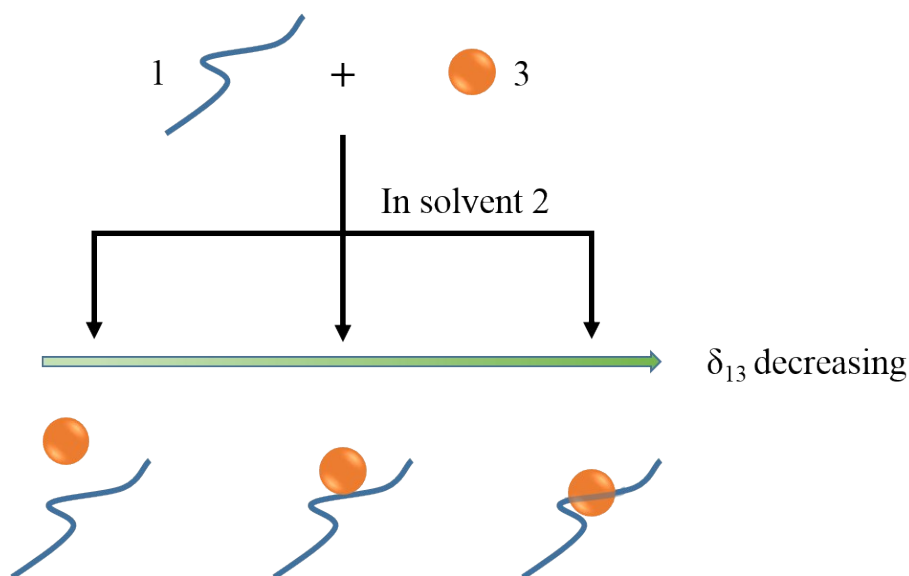


Figure S5. Schematics illustrating the difference ZIF-8 encapsulation results on β -MnO₂ NW under different interfacial energies.

In general, when combining two phases (1 and 3) in a solvent medium 2, three interfaces are formed, whose interfacial energies can be expressed as δ_{12} , δ_{23} and δ_{13} . Depending on their relative strength, if δ_{13} is large, the newly formed phase 3 cannot completely “wet” the nanowires surface, once δ_{13} value decreases, forming a 1-3 interface is favorable, and even 3 can engulf 1 if δ_{13} is low enough.¹ In our experiment, we calculated the δ_{13} between β -MnO₂ and ZIF-8 is 36.28 % (see Table 2 in the manuscript), which is much higher than the “wet” requirement (< 2 %).

The mismatches are calculated by the conventional definition given by *Shell Lattice Parameter – Core Lattice Parameter*

$$\frac{\text{Shell Lattice Parameter} - \text{Core Lattice Parameter}}{\text{Core Lattice Parameter}} \quad .^2$$

The major lattice planes of the core and shell components from XRD data are used in the calculation of the lattice mismatches.

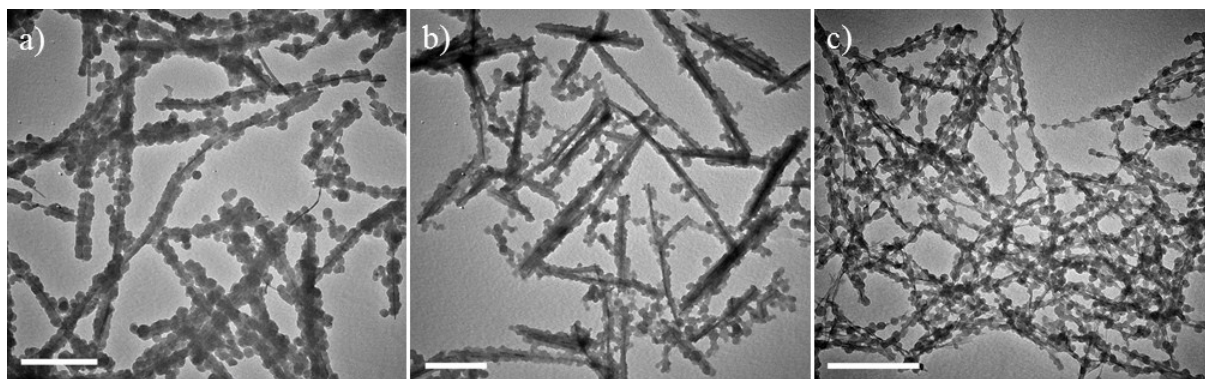


Figure S6. TEM image of the (a) MnOOH@ZIF-8, (b) α -MnO₂@ZIF-8 NWs and (c) TiO₂@ZIF-8 NWs. Scale bars: 500 nm.

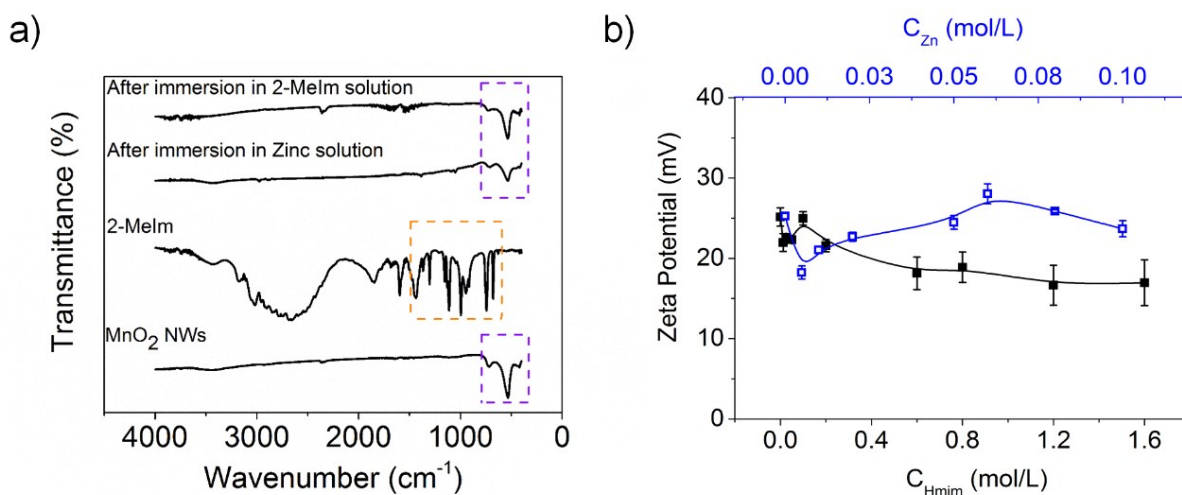


Figure S7. (a) Comparison of FTIR spectrum of β -MnO₂ NWs before and after immersing in separated zinc and 2-MeIm methanol solution for 2 h, respectively. (b) Zeta-potentials of β -MnO₂ NWs at different concentrations of zinc and 2-MeIm methanol solution, respectively.

In order to consider the chemical adsorption involved during the assembling process, we first conducted an experiment where immersing β -MnO₂ NWs in 2-MeIm methanol solution for 2 h. Compared to the characteristic peaks for pristine 2-MeIm (orange dashed box in Figure S7a), the surface functional groups of β -MnO₂ NWs showed a negligible change (purple dashed box). Besides, zeta potentials were measured for the alteration of surface charge densities, it was found that the surface charge remained stable after immersion in Figure S7b. In terms of zinc methanol solution, we consider that zinc ions were less likely to strongly coordinate with β -MnO₂ NWs because of the electrostatic repulsion between zinc and β -MnO₂ NWs (both are positive charge), and the results revealed a similar situation with that in 2-MeIm. Lastly, it is worth mentioning that no PVP prominent peaks were detected on β -MnO₂ NWs, meaning that PVP-effect is non-existed.

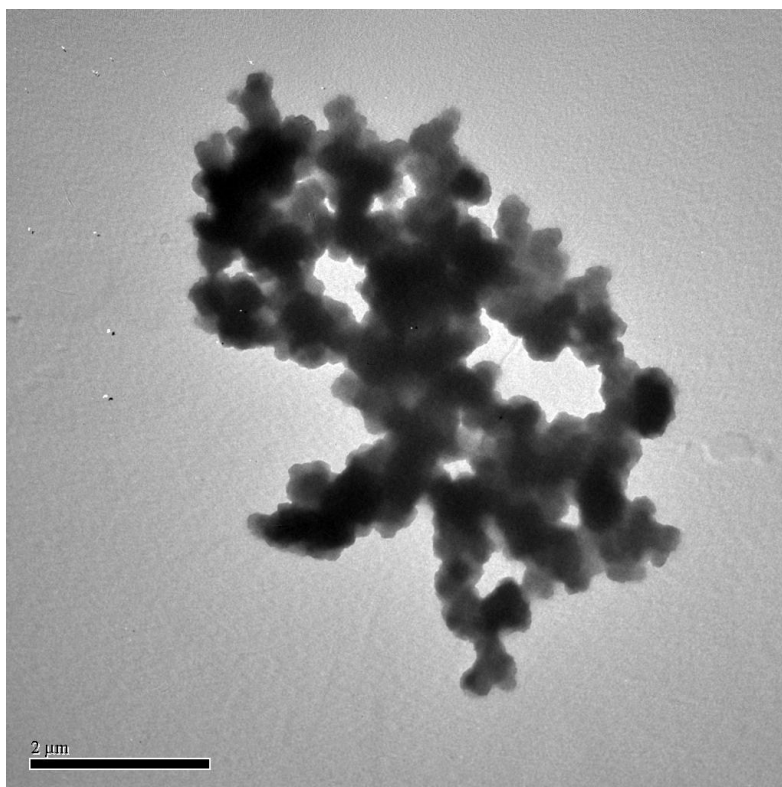


Figure S8. TEM image of ZIF-8 particles dispersed in the aqueous solution.

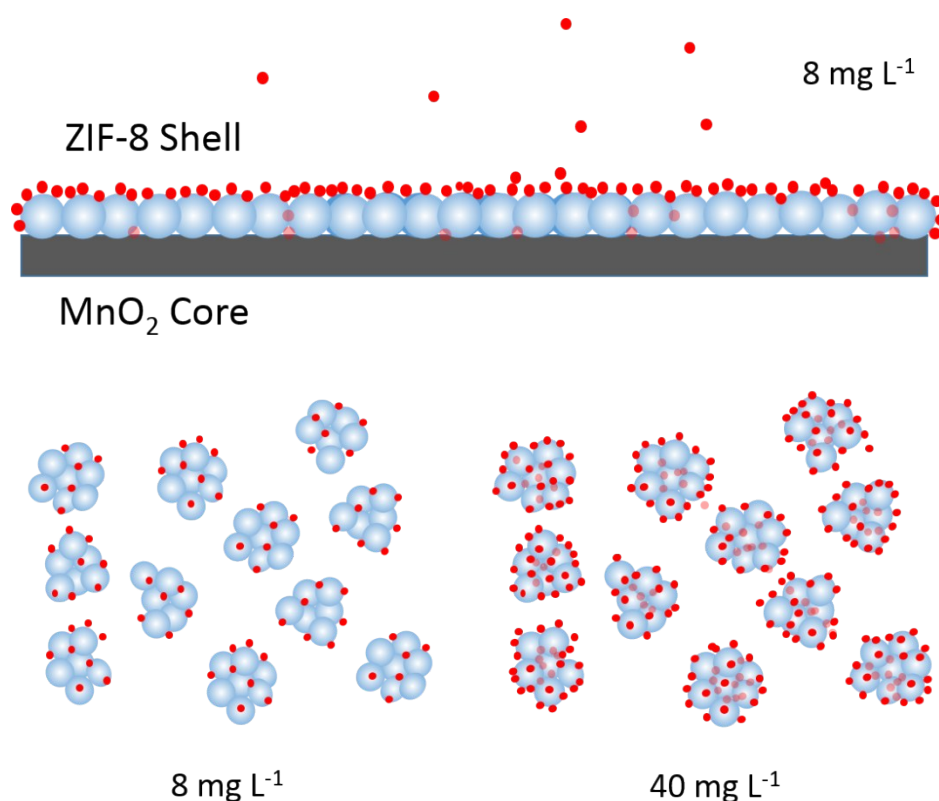


Figure S9. Schematic illustration of As(III) removal process on $\text{MnO}_2@\text{ZIF-8}$ NWs and ZIF-8 particles at different initial As(III) concentrations. Blue part represents ZIF-8 particles, red particles stand for As(III) ions.

In Figure S9, at a low As(III) concentration of 8 mg L^{-1} , As(III) ions first tend to transfer to the surface of adsorbents, and occupied the external binding sites. Nevertheless, ZIF-8 particles tend to agglomerate in water (Figure S8). This may block a large fraction of the adsorption sites of ZIF-8 in the inner matrix and affect the mass transportation. On the contrary, 1D structure of $\text{MnO}_2@\text{ZIF-8}$ NWs is beneficial to maintain a good dispersion along 1D MnO_2 NWs, resulting in adequate active sites were exposed. As a result, mass diffusion rate was promoted on $\text{MnO}_2@\text{ZIF-8}$ NWs. Compared to the pristine ZIF-8 adsorbent, the slower adsorption rate on $\text{MnO}_2@\text{ZIF-8}$ NWs at a high As(III) concentration of 40 mg L^{-1} is mainly because the exposed binding sites were occupied until saturation. And the pore apertures of continuous ZIF-8 barrier restrict As(III) ions diffused into inner core to some extent, despite of the defects may exist. However, for ZIF-8 matrix, the higher concentration gradient accelerated the mass diffusion into the intraparticle adsorption sites.

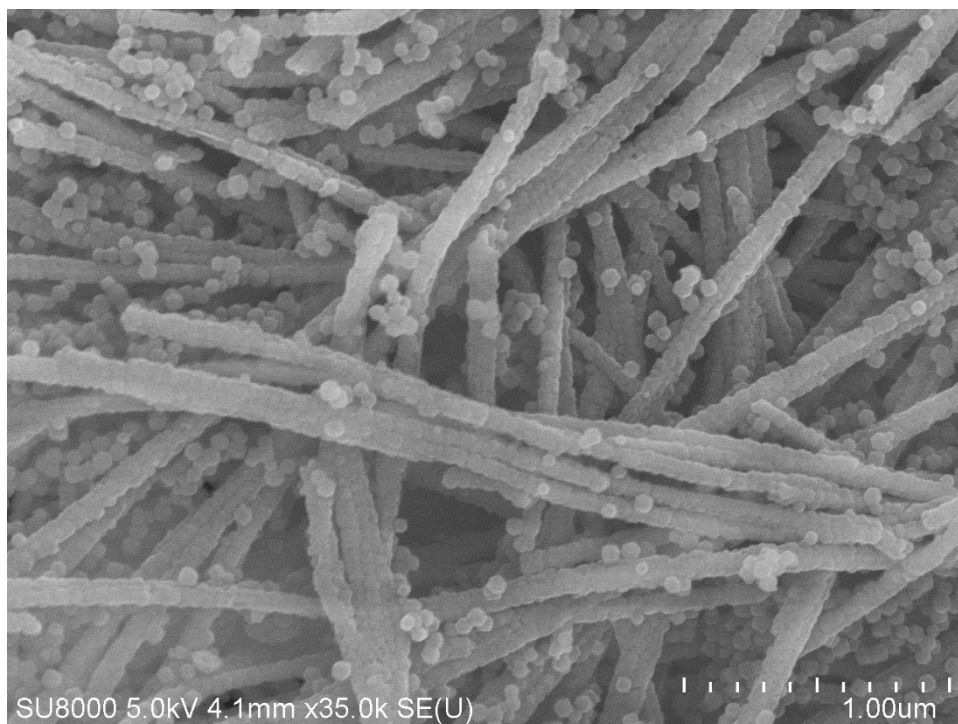


Figure S10. SEM image of $\text{MnO}_2@ZIF-8$ NWs after As(III) adsorption.

Table S1 ICP analyses for the MnO₂@ZIF-8 NWs with different ZIF-8 loadings.

MnO ₂ @ZIF-8 NWs	ZIF-8 content (wt. %)
Insufficient	24.21
Moderate	63.53
Excess	96.29

Table S2 The fitted parameters of Langmuir and Freundlich isotherms for As(III) on MnO₂, ZIF-8 and MnO₂@ZIF-8 adsorbents.

Adsorbents	Langmuir constants			Freundlich constants		
	Q_m	K_L	R^2	K_F	n^{-1}	R^2
	(mg/g)	(L/mg)		(mg/g)		
MnO ₂ NWs	14.31	0.186	0.994	5.090	0.239	0.910
ZIF-8	90.80	8.787	0.942	65.428	0.106	0.979
MnO ₂ @ZIF-8 NWs	140.27	0.388	0.981	42.25	0.311	0.946

Table S3 Parameters of adsorption kinetics for As(III) adsorption on ZIF-8 and MnO₂@ZIF-8 NWs adsorbents fitted by Pseudo-second-order kinetic model with different initial As(III) concentrations.

Adsorbents	8 mg L ⁻¹			40 mg L ⁻¹		
	q_e	V_0	R^2	q_e	V_0	R^2
	(mg g ⁻¹)	(g mg ⁻¹ h ⁻¹)		(mg g ⁻¹)	(g mg ⁻¹ h ⁻¹)	
ZIF-8	74.42	0.046	0.993	104.06	0.015	0.989
MnO ₂ @ZIF-8 NWs	69.47	0.061	0.999	137.89	0.007	0.998

References

1. Sun, H.; He, J.; Wang, J.; Zhang, S.-y.; Liu, C.; Sritharan, T.; Mhaisalkar, S.; Han, M.-Y.; Wang, D.; Chen, H., *J. Am. Chem. Soc.*, **2013**, *135*, 9099-9110.
2. Zhang, J., Tang, Y., Lee, K., Ouyang, M., *Science*, **2010**, *327*, 1634-1638.